Three-dimensional Josephson-junction arrays: Static magnetic response

R. De Luca and T. Di Matteo
INFM-Dipartimento di Fisica, Universita' degli Studi di Salerno, I-84081 Baronissi (Salerno), Italy

A. Tuohimaa and J. Paasi
Laboratory of Electricity and Magnetism, Tampere University of Technology, FIN-33101 Tampere, Finland
(Received 17 July 1997)

In this work we present a simple three-dimensional Josephson-junction array model: a cube with twelve junctions, one on each edge. The low-field magnetic response of the system is studied numerically for arbitrary directions of the applied field. In this model the magnetic energy of the circulating currents is taken into account by introducing an effective mutual inductance matrix. The lower threshold field for flux penetration is determined in a closed analytic form for field directions perpendicular to one cube side.
[S0163-1829(98)05502-7]

I. INTRODUCTION

The interest in Josephson-junction arrays has been constantly growing since the discovery of high-T_c superconductors.[1] Indeed, it was soon clear that the low-field electromagnetic properties of this class of superconductors could be well described by means of Josephson junction networks.[2,3]

The study of the physical properties of one-dimensional (1D), two-dimensional (2D), and three-dimensional (3D) arrays of Josephson junctions, though, started before the advent of high-T_c superconductivity. Nakajima and Sawada,[4] for example, had already derived the dynamical equations for flux motion in infinite 2D and 3D arrays of inductively coupled small Josephson junctions in 1981. In a somewhat more restrictive scenario, other authors were at the time studying the dynamical properties of these systems for negligible magnetic energy of the circulating currents.[5,6] Recently, a closer link between the low-field static magnetic properties of 2D and 3D arrays of inductively coupled small Josephson junctions and the corresponding phenomenological quantities of high-T_c granular superconductors has been attempted by many authors.[7–10] However, the properties of 3D Josephson-junction arrays have not been investigated in depth yet. Indeed, only few recent works on the subject have appeared in the literature.[11,12]

In the present work we study the static magnetic properties of the simple 3D network shown in Fig. 1 consisting of twelve inductively coupled small Josephson junctions. In the following section we start by showing that this system is indeed an appropriate model for a physical system consisting of eight grains in a cubic arrangement. In Sec. III we write the dynamical equations that govern flux transitions in the cubic network for an arbitrary direction of the applied field. In Sec. IV the flux and current distributions are found by numerically integrating the dynamical equations derived in the previous section. In Sec. V the lower threshold field for flux transitions in the system after zero-field cooling (ZFC) is derived in a closed analytic form for applied fields perpendicular to one of the cube side. Conclusions are drawn in the last section.

II. THE PHYSICAL SYSTEM

In the present section we show that the network in Fig. 1 could be considered to be a model circuit of the physical system shown in Fig. 2, consisting of eight superconducting grains in a cubic arrangement. Let us then start by associating a Josephson junction (JJ) to each contact point between adjacent grains in Fig. 2. We immediately see that the resulting model network must contain twelve JJ's. To each JJ one associates a gauge invariant superconducting phase difference $\varphi_\xi(\mathbf{r})$ where $\mathbf{r}=(x,y,z)$ denotes the position of the junction and ξ is the direction along which the junction lies. It is well known that the dynamical equations for the φ_ξ's can be derived with the aid of the resistively shunted junction model[13] once the current circulating in the junction is known. In order to understand the connection between the physical currents circulating in the system of Fig. 2 and those circulating in the model system of Fig. 1, let us first consider the simplest case of an external magnetic field of amplitude H in the z direction. In this case, the most general current distribution is represented in Fig. 3. This current distribution is due to the axial symmetry of the problem and consists of currents $i_{\rm up}$ and $I_{\rm up}$ flowing in the inner and outer upper loops, respectively, and of currents $i_{\rm low}$ and $I_{\rm low}$ flowing in the corresponding lower loops. In the case the external field is along an arbitrary direction in space, we may represent the whole current distribution in the system by means of the currents $i_{(\eta\xi)}(\mathbf{r})$ and $I_{(\eta\xi)}(\mathbf{r})$, which are taken to be the inner and outer loop currents flowing in the η-ξ plane at position $\mathbf{r}$. The currents circulating in a given face are taken to be positive when seen to circulate in the counterclockwise direction by an external observer placed at infinity on the positive side of the axis orthogonal to the face itself. By assuming spatial homogeneity of the system, we could express the fluxes in terms of the circulating current by introducing the complete inductance matrix, whose structure could be summarized as follows:

$$\mathcal{M}^{(\mu\nu)}_{(\eta\xi)}(\mathbf{r},\mathbf{r}')=[\,\delta_{\mathbf{r},\mathbf{r}'}L+(1-\delta_{\mathbf{r},\mathbf{r}'})M]\,\delta_{(\mu\nu),(\eta\xi)} +[-1]^{(\delta_{\mathbf{r},\mathbf{r}'})}M_0[1-\delta_{(\mu\nu),(\eta\xi)}], \quad (1)$$

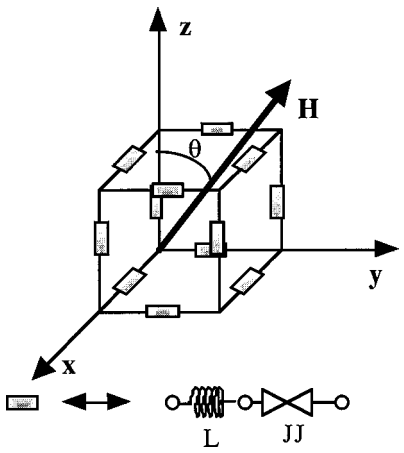

FIG. 1. The circuit model: Each box contains an inductor and a Josephson junction, as shown in the inset.

$$\mathcal{N}^{(\mu\nu)}_{(\eta\xi)}(\mathbf{r},\mathbf{r}') = [\,\delta_{\mathbf{r},\mathbf{r}'} l + (1-\delta_{\mathbf{r},\mathbf{r}'})m\,]\,\delta_{(\mu\nu),(\eta\xi)} + [-1]^{(\delta_{\mathbf{r},\mathbf{r}'})} m_0 [1-\delta_{(\mu\nu),(\eta\xi)}], \tag{2}$$

$$\mathcal{K}^{(\mu\nu)}_{(\eta\xi)}(\mathbf{r},\mathbf{r}') = [\,\delta_{\mathbf{r},\mathbf{r}'} m^* + (1-\delta_{\mathbf{r},\mathbf{r}'})m'\,]\,\delta_{(\mu\nu),(\eta\xi)} + [-1]^{(\delta_{\mathbf{r},\mathbf{r}'})} m_0' [1-\delta_{(\mu\nu),(\eta\xi)}], \tag{3}$$

where the elements of the matrix $\mathcal{M}$ are relative to outer-outer loop current interactions, those of the matrix $\mathcal{N}$ pertain to inner-inner loop current interactions, and those of the matrix $\mathcal{K}$ pertain to inner-outer loop current interactions. In addition, the vectors $\mathbf{r}$ and $\mathbf{r}'$ here represent the position of the unit cell for the system, consisting of three faces in the three planar orientations in space, namely, (yz), (xz), and (xy), as shown in Fig. 4. The double greek indices are taken to represent in a concise way all these three orientations. Furthermore, the coefficients L and l represent the self-inductance of the outer and inner loops, respectively. The set of coefficients M, m, and m' and the set M_0, m_0, and m_0' are the mutual inductance coefficients between parallel and orthogonal faces, respectively. Finally, the coefficient m^* represents the mutual coupling between inner and outer currents lying on the same cube side.

The fluxes linked the inner and outer loops lying in the η-ξ plane at position $\mathbf{r}$, denoted by $\Phi_{(\eta\xi)}(\mathbf{r})$ and $\Theta_{(\eta\xi)}(\mathbf{r})$, respectively, could be thus written in the following compact form:

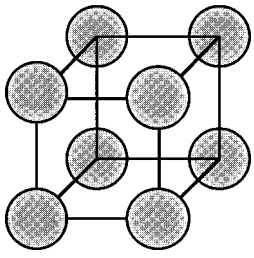

FIG. 2. The physical system: Eight weakly-coupled superconducting grains in a cubic arrangement.

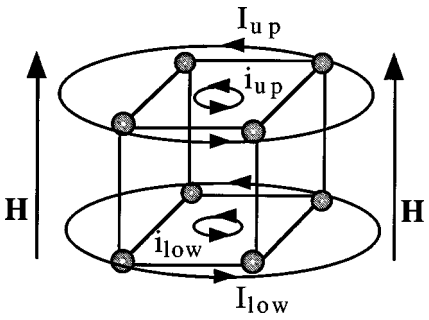

FIG. 3. Most general current distribution for the physical system represented in Fig. 2 when a magnetic field in the vertical direction is applied.

$$\Phi_{(\eta\xi)}(\mathbf{r}) = \sum_{\mathbf{r}'}\sum_{\mu\nu} \mathcal{K}^{(\mu\nu)}_{(\eta\xi)}(\mathbf{r},\mathbf{r}') I_{(\mu\nu)}(\mathbf{r}') + \sum_{\mathbf{r}'}\sum_{\mu\nu} \mathcal{M}^{(\mu\nu)}_{(\eta\xi)}(\mathbf{r},\mathbf{r}') i_{(\mu\nu)}(\mathbf{r}') + \mu_0 \mathbf{H}\cdot\mathbf{s}_{(\eta\xi)}(\mathbf{r}), \tag{4}$$

$$\Theta_{(\eta\xi)}(\mathbf{r}) = \sum_{\mathbf{r}'}\sum_{\mu\nu} \mathcal{M}^{(\mu\nu)}_{(\eta\xi)}(\mathbf{r},\mathbf{r}') I_{(\mu\nu)}(\mathbf{r}') + \sum_{\mathbf{r}'}\sum_{\mu\nu} \mathcal{K}^{(\mu\nu)}_{(\eta\xi)}(\mathbf{r},\mathbf{r}') i_{(\mu\nu)}(\mathbf{r}') + \mu_0 \mathbf{H}\cdot\mathbf{S}_{(\eta\xi)}(\mathbf{r}), \tag{5}$$

where $\mathbf{S}_{(\eta\xi)}$ and $\mathbf{s}_{(\eta\xi)}$ are the area vectors pertaining to the outer and inner loops orthogonal to the η-ξ plane, respectively. By assuming the grains to be in the perfect Meissner state, we can write:

$$\Phi_{(\eta\xi)}(\mathbf{r}) = \Theta_{(\eta\xi)}(\mathbf{r}). \tag{6}$$

Finally, by solving Eqs. (4) and (5) with the conditions given by Eqs. (6), one can express the flux linked to either the outer or the inner loop in a single planar direction in terms of the effective currents circulating in the twelve junctions, namely, the currents $I^{(B)}_{(\eta\xi)}(\mathbf{r}) = I_{(\eta\xi)}(\mathbf{r}) + i_{(\eta\xi)}(\mathbf{r})$, and in terms of effective self- and mutual-inductance parameters. We have thus established that the network in Fig. 1 can be seen as the circuit equivalent of a system of eight superconducting grains as shown in Fig. 2. Therefore, in adopting a

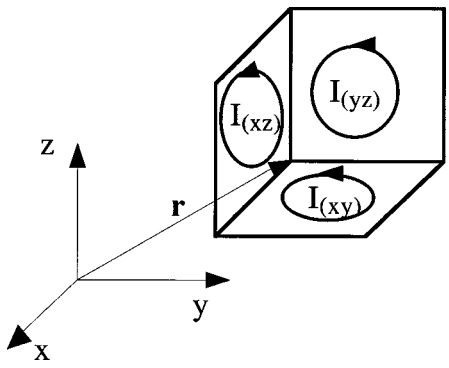

FIG. 4. Schematic representation of the current variables for a single unit of mutually orthogonal faces in the cubic network.

3D network as a model of a real system, whose electromagnetic properties are to be studied, one should bear in mind that the currents depicted in the circuit of Fig. 1 describe only the currents that effectively flow into the junctions, so that the current distribution of Fig. 1 does not reproduce the actual current distribution of the physical system, like, for example, the one depicted in Fig. 3. However, the complete treatment of the physical system is rather difficult since the shielding currents circulating at the grain surfaces are not easy to calculate and only a portion of the superficial current density flows through the junctions. Therefore, we shall only consider the simple case of the network shown in Fig. 1, in which the external and the internal current loops have the same values of inductances and thus $\mathcal{M}^{(\mu\nu)}_{(\eta\xi)}(\mathbf{r},\mathbf{r}') = \mathcal{N}^{(\mu\nu)}_{(\eta\xi)}(\mathbf{r},\mathbf{r}') = \mathcal{K}^{(\mu\nu)}_{(\eta\xi)}(\mathbf{r},\mathbf{r}')$. The notation to be used hereafter is consistent with the inner loop notation.

Each face of the cube in Fig. 1 contains a square current loop made of thin cylindrical wire of diameter $2r$, the side length being a. The self-inductance of the loop is given by[14,15]

$$l = \frac{\mu_0 a}{4\pi}\left[2 + 8\left(\ln\frac{2a}{r(1+\sqrt{2})} + \sqrt{2} - 2\right)\right]. \tag{7}$$

All the current loops can be divided into perpendicular and parallel components. In the Neuman formula[15] the perpendicular components vanish and, therefore, it is useful to cut the circulation integrals of the Neuman formula into pieces dealing with two parallel current blocks at the time. This leads to partial mutual inductance

$$m_{par} = \frac{\mu_0}{4\pi}\int_0^a\int_0^a \frac{dl_1 dl_2}{\sqrt{(l_1-l_2)^2+d^2}} = \frac{\mu_0}{4\pi}\left[2d - 2\sqrt{a^2+d^2} + 2a\,\sinh^{-1}(a/d)\right], \tag{8}$$

where d ($=a$ or $\sqrt{2}a$) is the distance between the parallel blocks. The directions of the currents in the blocks are taken into account by setting the $m_{\rm par}$ as positive for equal current directions and negative for opposite directions. The circulation integrals of the Neuman formula are completed by using the corresponding $m_{\rm par}$'s. In this way, we obtain mutual inductance of the orthogonal loops as

$$m_0 = -\,l/4 + 0.02\mu_0 a, \tag{9}$$

where $l/4$ comes from galvanic connection in the one-loop side. Similarly, the mutual inductance of the parallel current loops is

$$m = 0.08\mu_0 a. \tag{10}$$

III. THE MODEL EQUATIONS

One possible way of labeling the phase variables is to refer to the position in space $\mathbf{r}=(x,y,z)$ of the corresponding JJ's and to the direction along which the junctions lie, as already specified before. Since the position vector $\mathbf{r}$ has been taken, in the previous section, to correspond to the position of the origin $O(\mathbf{r})$ of the unit cell shown in Fig. 4, we denote by $\varphi_x(\mathbf{r})$, $\varphi_y(\mathbf{r})$, and $\varphi_z(\mathbf{r})$ the phase of the junctions which are closer to $O(\mathbf{r})$ and which lie in the x, y, and z direction, respectively. The phase variables of the six still unlabeled junctions in Fig. 4 can be expressed as $\varphi_\xi(\mathbf{r}+a\hat{\eta})$, where the direction $\hat{\eta}$ is different from the direction $\hat{\xi}$.

Currents and fluxes, on the other hand, can be labeled through a standard tensorial notation, as seen in the previous section. In this way, the quantities $I^B_{(xy)}(\mathbf{r})$ and $I^B_{(xy)}(\mathbf{r}+a\hat{z})$ denote the loop currents seen to flow in the counterclockwise direction by an external observer placed on the positive z axis. The first current circulates in a cube face placed right on the x-y plane, the second in a face translated by a length a in the z direction. The corresponding fluxes can thus be written as $\Phi_{(xy)}(\mathbf{r})$ and $\Phi_{(xy)}(\mathbf{r}+a\hat{z})$. By imposing fluxoid quantization to each closed loop of the network, one can write the six relations between the normalized flux variables $\Psi=\Phi/\Phi_0=\Theta/\Theta_0$ and the superconducting phases

$$2\pi\Psi_{(yz)}(\mathbf{r}) = 2\pi n_{(yz)}(\mathbf{r}) - \varphi_y(\mathbf{r}+a\hat{z}) + \varphi_y(\mathbf{r}) + \varphi_z(\mathbf{r}+a\hat{y}) - \varphi_z(\mathbf{r}), \tag{11}$$

$$2\pi\Psi_{(xz)}(\mathbf{r}) = 2\pi n_{(xz)}(\mathbf{r}) - \varphi_z(\mathbf{r}+a\hat{x}) + \varphi_z(\mathbf{r}) + \varphi_x(\mathbf{r}+a\hat{z}) - \varphi_x(\mathbf{r}), \tag{12}$$

$$2\pi\Psi_{(xy)}(\mathbf{r}) = 2\pi n_{(xy)}(\mathbf{r}) - \varphi_x(\mathbf{r}+a\hat{y}) + \varphi_x(\mathbf{r}) + \varphi_y(\mathbf{r}+a\hat{x}) - \varphi_y(\mathbf{r}). \tag{13}$$

In the same way the fluxoid quantization equations can be written for the other loops contained in the remaining three cube faces by introducing a translation operator $\hat{T}_\eta$, where the index η gives the direction along which the translation is performed. This operator acts directly upon the position vector $\mathbf{r}$. For example, when applied to the phase variables it acts in the following way:

$$\hat{T}_\eta\varphi_\xi(\mathbf{r}) = \varphi_\xi(\mathbf{r}+a\hat{\eta}). \tag{14}$$

The same is true for the fluxes $\Psi_{(\mu\nu)}(\mathbf{r})$, the currents $I_{(\mu\nu)}(\mathbf{r})$ and the flux numbers $n_{(\mu\nu)}(\mathbf{r})$. The flux variables are also linked to the loop currents and to the externally applied field $\mathbf{H}$ according to the following:

$$\Phi_{(\eta\xi)}(\mathbf{r}) = \sum_{\mathbf{r}'}\sum_{\mu\nu} A^{(\mu\nu)}_{(\eta\xi)}(\mathbf{r},\mathbf{r}')I^B_{(\mu\nu)}(\mathbf{r}') + \mu_0\mathbf{H}\cdot\mathbf{S}^{\rm eff}_{(\eta\xi)}(\mathbf{r}), \tag{15}$$

where $\mathbf{S}^{\rm eff}_{(\eta\xi)}(\mathbf{r})$ is the effective area vector pertaining to the cube face orthogonal to the η-ξ plane and $A^{(\mu\nu)}_{(\eta\xi)}(\mathbf{r},\mathbf{r}')$ are effective mutual inductance coefficients.

Introducing the nonlinear Josephson operator O_J, defined as

$$O_J(\cdot) = \frac{\Phi_0}{2\pi R}\frac{d}{dt}(\cdot) + I_J\sin(\cdot), \tag{16}$$

where the resistive parameter R is taken to be the same for all JJ's and where the quantity I_J is the maximum Josephson current of the junctions. The quantity I_J should carry information on the position of the junction; nevertheless, we omit these extra indices to keep the notation simpler. The equations of the motion for the twelve phase variables can be thus written as follows:

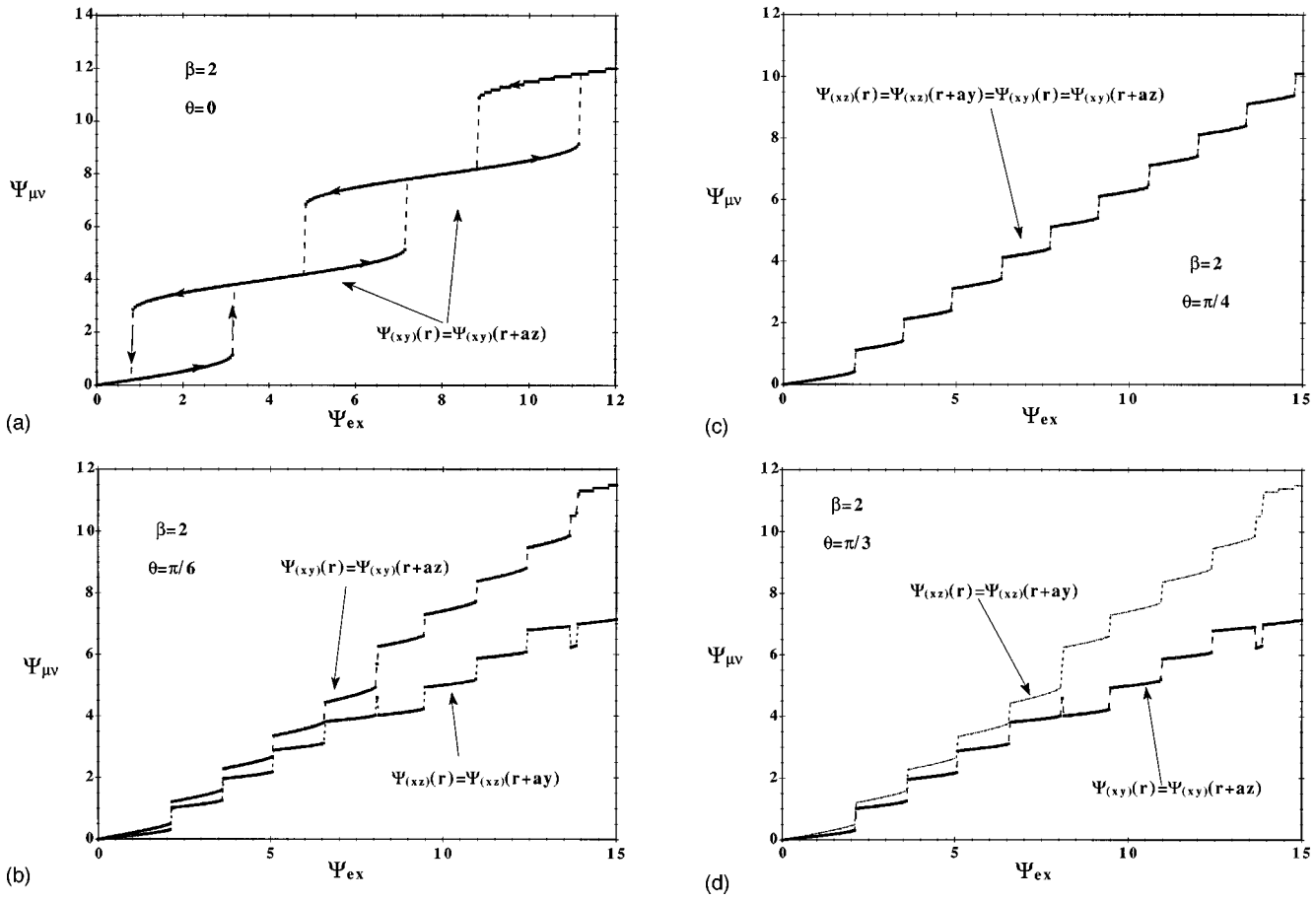

FIG. 5. Flux linked to the six cubic faces as a function of the normalized applied flux Ψ_{ex} for $\beta=2.0$ and for various field orientations: (a) $\theta=0$; (b) $\theta=\pi/6$; (c) $\theta=\pi/4$; (d) $\theta=\pi/3$. In Fig. 5(a) we let Ψ_{ex} vary in a cicle in the interval [0,12]. In Figs. 5(b)–5(d) Ψ_{ex} is taken to increase from 0 to 15.

$$O_J[\varphi_\xi(\mathbf{r})]=\sum_{\mu\nu}\epsilon_{\xi\mu\nu}[I^B_{(\xi\nu)}(\mathbf{r})-I^B_{(\xi\nu)}(\mathbf{r}-a\hat{\nu})], \quad (17)$$

where $\epsilon_{\xi\mu\nu}$ is the Levi Civita symbol. The above set of nonlinear ordinary differential equations applies in general to a 3D cubic array of Josephson junctions and must be specialized to the single cube case by taking care of setting to zero all the currents that are not present in the system.

In order to solve the above set of equations, it is necessary to express the currents appearing on the right-hand side of Eqs. (17) in terms of the flux numbers Ψ, which, in turn, are to be expressed in terms of the phase variables through Eqs. (11)–(13). In this way, the dynamical equations (17) become a set of twelve coupled nonlinear differential equations in the phase variables φ_ξ's. By numerically integrating this set of equations and by recalling Eqs. (11)–(13) and Eqs. (15) one can determine the magnetic properties of the model.

IV. STATIONARY MAGNETIC STATES AFTER ZFC

Having derived the dynamical equations for the system, we may now determine the stationary magnetic states after ZFC. We integrate the resulting set of nonlinear coupled differential equations [Eqs. (17)] by giving a null initial value to all phase variables φ_ξ's under the forcing condition of zero applied magnetic field **H**. Subsequently, we give a small enough variation $\Delta\mathbf{H}$ to the applied field in a fixed direction in space and let the system evolve to a new equilibrium state compatible with the new forcing condition $\mathbf{H}=\Delta\mathbf{H}$. Finally, starting from this new state, we apply the same procedure repeatedly, until a maximum value of the applied field strength is reached. The way in which we determine the stationary magnetic states of the system thus relies upon the numerical solution of the dynamical equations, which link a metastable magnetic state realized at a given value of externally applied field **H** to one at $\mathbf{H}+\Delta\mathbf{H}$.

Once the phase variables are obtained for increasing applied field strengths in a fixed direction in space, the flux distribution can be obtained by Eqs. (11)–(13), and the current distribution can be derived from Eqs. (15) by inverting the mutual inductance matrix $A^{(\mu\nu)}_{(\eta\xi)}(\mathbf{r},\mathbf{r}')$. In order to carry out numerical results, one should first estimate the values of the model parameters. The most important one for networks of inductively coupled Josephson junctions is undoubtedly the generalized superconducting quantum interference device (SQUID) parameter $\beta=lI_J/\Phi_0$. By making use of Eqs. (7)–(10), for $a=10$ μm and $a/r=10^2$ we find $l=3.3\times10^{-7}$ H, $m/l=0.03$, and $m_0/l=-0.24$. Therefore, for maximum Josephson current values of the order of 100 μA, the adimensional generalized SQUID parameter can be estimated to be of the order of unity. In the present paper we take $\beta=2$ throughout. The resulting flux and current distributions in the system are shown in Figs. 5(a)–5(d) through Figs. 8(a)–8(d).

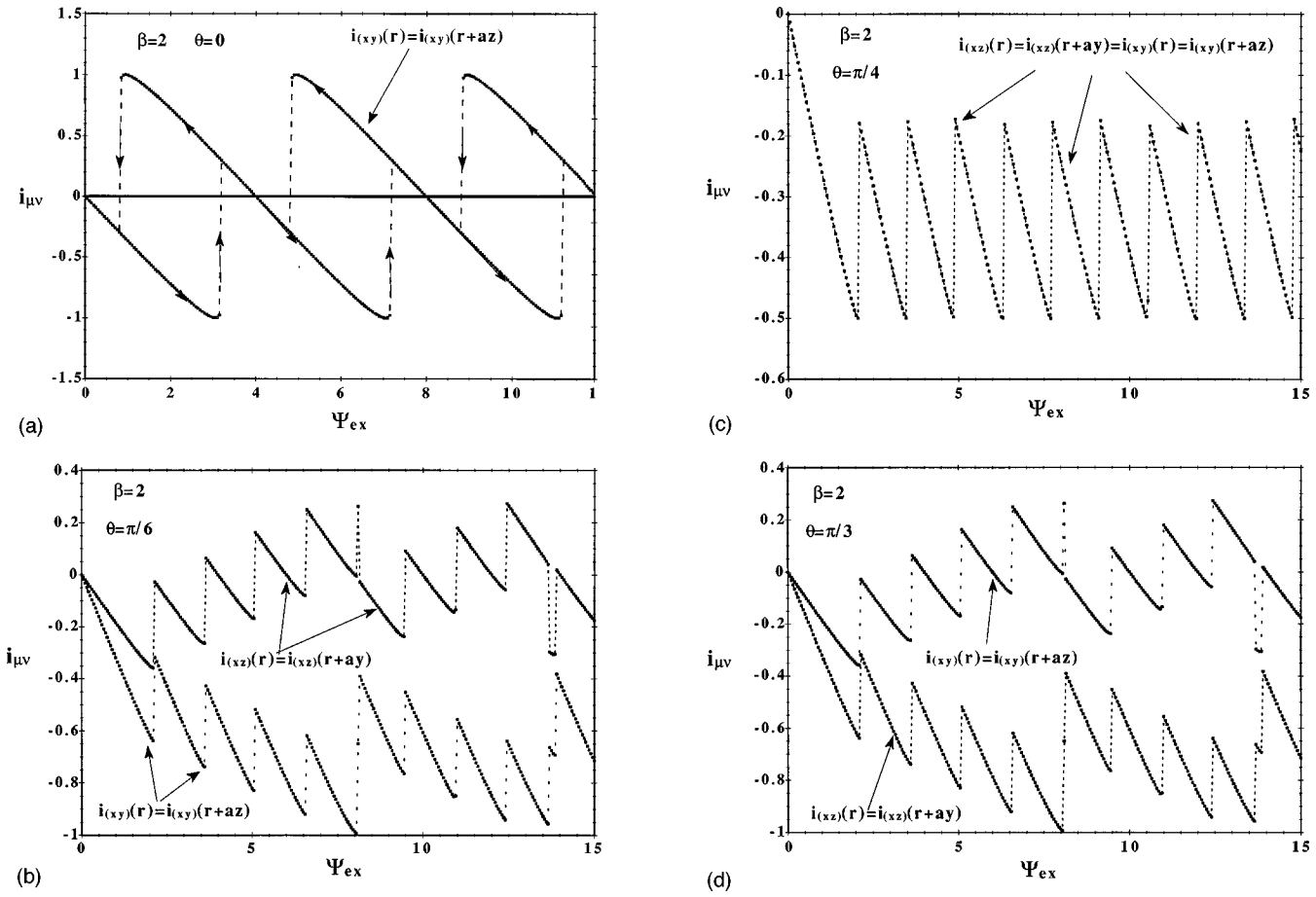

FIG. 6. Mesh currents circulating in the six cubic faces as a function of the normalized applied flux Ψ_{ex} for $\beta=2.0$ and for various field orientations: (a) $\theta=0$; (b) $\theta=\pi/6$; (c) $\theta=\pi/4$; (d) $\theta=\pi/3$. In Fig. 6(a) we let Ψ_{ex} vary in a cicle in the interval [0,12]. In Figs. 6(b)–6(d) Ψ_{ex} is taken to increase from 0 to 15.

In Figs. 5(a)–5(d) and in Figs. 6(a)–6(d) the normalized fluxes $\Psi_{\mu\nu}$ and the normalized currents $i_{\mu\nu}=I_{\mu\nu}/I_{J0}$ are plotted, respectively, in terms of the normalized forcing term $\Psi_{ex}=\mu_0 H S_0^{\rm eff}/\Phi_0$, for identical junctions, all with maximum Josephson current equal to I_{J0} and taken to be field-independent for simplicity. In Figs. 7(a)–7(d) and Figs. 8(a)–(d), the normalized flux and currents are reported in terms of Ψ_{ex} for junctions with a distribution of the parameter differences (I_J-I_{J0}) peaked about a null mean value. In Figs. 5(a) and 6(a) the magnetic field is applied in a direction perpendicular to the base of the cubic network, while in Figs. 5(b)–5(d) and in Figs. 6(b)–6(d) the field direction is taken at an angle θ with respect to the z axis [(a) $\theta=\pi/6$, (b) $\theta=\pi/4$, (c) $\theta=\pi/3$]. The same is true for Figs. 7(a)–7(d) and Figs. 8(a)–8(d). Let us first comment the results obtained for identical junctions. In the graphs in Figs. 5(a)–(d) we notice the appearance of lower threshold Ψ_{ex} values for irreversible flux penetration, which we shall here denote as $\Psi_{ex}^{(1)}$. Indeed, for normalized applied fluxes lower than $\Psi_{ex}^{(1)}$, the $\Psi_{\mu\nu}$ vs Ψ_{ex} curves are seen to follow a reversible path, starting from ZFC. At $\Psi_{ex}=\Psi_{ex}^{(1)}$ an irreversible flux transition involving four flux quanta occurs. A discontinuity in the current distributions corresponding to the $\Psi_{ex}=\Psi_{ex}^{(1)}$ values can be noticed in Figs. 6(a)–6(d). The presence of hysteresis in the system can be readily verified by looking at Figs. 5(a) and 6(a), in which we have cycled Ψ_{ex} in the interval [0, 12]. The same type of behavior is also present for different field directions; for the sake of clarity, however, in the rest of the figures we have only shown results for increasing Ψ_{ex} values. In particular, in the following section it will be shown that the cubic system, in the case of $\theta=0$, acts much like a SQUID, so that $\Psi_{ex}^{(1)}$ can be analytically determined. In general, then, for $\Psi_{ex}>\Psi_{ex}^{(1)}$ a new magnetic state appears. The number of fluxons trapped in the system will be almost unaltered until a new flux transition occurs at $\Psi_{ex}^{(2)}$, where discontinuities can be detected in the current distributions. Successive flux transition will show a periodic behavior in the applied flux Ψ_{ex}. We may notice that, while for $\theta=0$ the flux linked to the side loops is zero, in the case the angle θ is different from zero this condition is not verified. As a consequence, the flux distribution may differ considerably in the two cases. Indeed, as the angle θ increases, flux penetration mechanisms, which in Fig. 5(a) and Fig. 6(a) pertained only to the x-y plane are gradually transferred to the x-z plane, in the following way: For $\theta=0$ all fluxons penetrating the system are aligned to the z axis, given the axial field symmetry. For applied field angles θ different from zero, one envisions a penetration mechanism that is due to the superposition of the two field components, one along z, one along x. The fluxons thus penetrate the faces in the x-y or x-z plane in such a way that the combination of the number of fluxons along z and those along x gives an asymptotic field direction

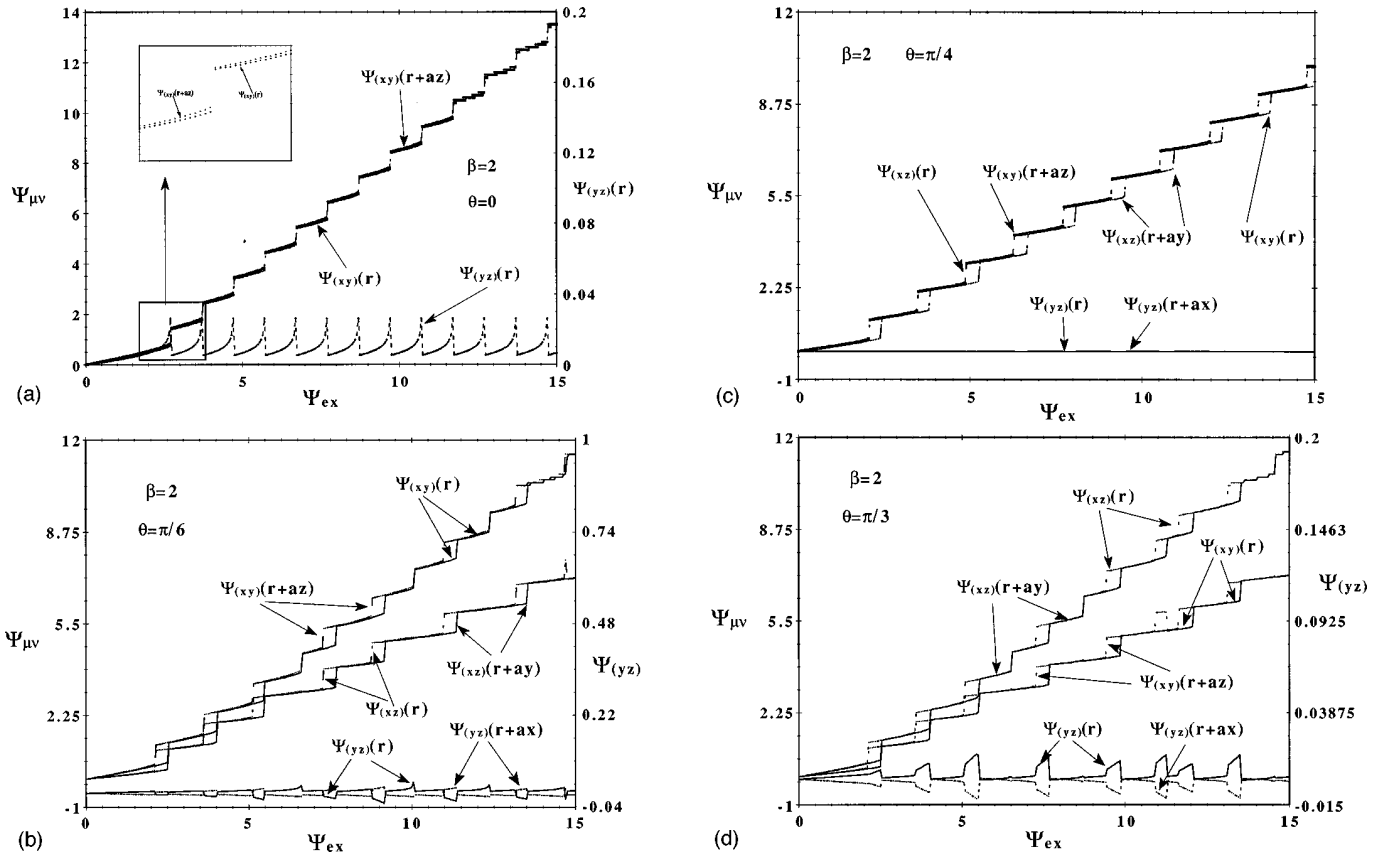

FIG. 7. Flux linked to the six cubic faces as a function of the normalized applied flux Ψ_{ex} for nonidentical junctions. The average SQUID parameter is $\beta=2.0$ and the maximum Josephson currents have a peaked distribution about the mean. Four runs have been done for the following field orientations: (a) $\theta=0$; (b) $\theta=\pi/6$; (c) $\theta=\pi/4$; (d) $\theta=\pi/3$. The external field Ψ_{ex} is taken to increase from 0 to 15.

equal to that of the applied field. As an example, when $\theta=\pi/4$, only two of the four fluxons entering the system during a flux transition penetrate through the x-y plane, the other two penetrate through the x-z plane. Following the same type of reasoning, for $\theta=\pi/2$, all penetrated fluxons must penetrate through the x-z plane. In these cases, the asymptotic condition is satisfied at the very beginning of the irreversible penetration process. On the other hand, for noncommensurate values of the ratio of the applied flux components ($\theta=\pi/6$ and $\theta=\pi/3$), the asymptotic condition is met at relatively high-field values.

In the case of nonidentical junctions, instead, single fluxons penetrate the superconducting network. This, of course, is a clear effect of the presence of inhomogeneity in the junction parameters, which is a situation closer to what can be observed in physical systems. Indeed, when an external magnetic field is applied to a superconducting network after ZFC, shielding currents $I_{\mu\nu}$ circulate in the system. However, some branch current, given by shielding current differences, may exceed the maximum Josephson current of one of the junctions with a weaker coupling energy, so that a single flux transition appears because of a 2π phase slip in this junction. The current distribution thus suffers a discontinuous change to a new configuration where another weakly coupled junction may allow a fluxon into the network when the external field is further increased. In this way, smoother but rather more difficult to follow transitions appear, as shown in Figs. 7(a)–7(d) and Figs. 8(a)–8(d).

Take, as a first example, flux transitions occurring for an external field applied in the axial direction [Figs. 7(a) and 8(a)]. We chose the junction strengths to be as follows: $i_{Jx}(\mathbf{r})=1.05$, $i_{Jx}(\mathbf{r}+a\hat{y})=1.10$, $i_{Jx}(\mathbf{r}+a\hat{z})=1.00$, $i_{Jx}(\mathbf{r}+a\hat{y}+a\hat{z})=0.95$, $i_{Jy}(\mathbf{r})=0.95$, $i_{Jy}(\mathbf{r}+a\hat{x})=1.00$, $i_{Jy}(\mathbf{r}+a\hat{z})=0.90$, $i_{Jy}(\mathbf{r}+a\hat{x}+a\hat{z})=0.95$, $i_{Jz}(\mathbf{r})=1.00$, $i_{Jz}(\mathbf{r}+a\hat{x})=1.05$, $i_{Jz}(\mathbf{r}+a\hat{y})=1.00$, $i_{Jz}(\mathbf{r}+a\hat{x}+a\hat{y})=1.05$, where $i_{J\xi}(\mathbf{r})$ is the normalized value of the maximum Josephson current of the junction placed at $\mathbf{r}$ and lying in the direction ξ. The weakest junction in the faces lying in the x-y plane, where the highest values of the screening currents are present, is the one with maximum Josephson current $i_{Jy}(\mathbf{r}+a\hat{z})=0.90$. This JJ is located on the common edge of the upper base and the back face in the y-z plane and can be denoted, by extending the notation used before, as $\mathrm{JJ}_y(\mathbf{r}+a\hat{z})$. Because of inhomogeneity, the flux in the latter face is not zero, as it is shown, by means of an enlarged scale, in the lower part of Fig. 7(a). This extra flux links to the upper base face, so that $\Psi_{xy}(\mathbf{r}+a\hat{z})$ is always greater than $\Psi_{xy}(\mathbf{r})$, as shown in the same Fig. 7(a). This asymmetry grows larger and larger until phase slip of the weakest junction in the upper base face, namely the junction $\mathrm{JJ}_y(\mathbf{r}+a\hat{z})$, and a successive phase slip of the weakest junction in the lower base face [$\mathrm{JJ}_y(\mathbf{r})$] do not reduce the difference between $\Psi_{xy}(\mathbf{r}+a\hat{z})$ and $\Psi_{xy}(\mathbf{r})$. Notice also how the flux jump is of almost one flux quantum. A similar analysis can be done even in the noncommensurate applied field components. However, the flux and current distributions are more complex, as it is evident from Figs. 7(b) and 7(d) and Figs. 8(b) and 8(d).

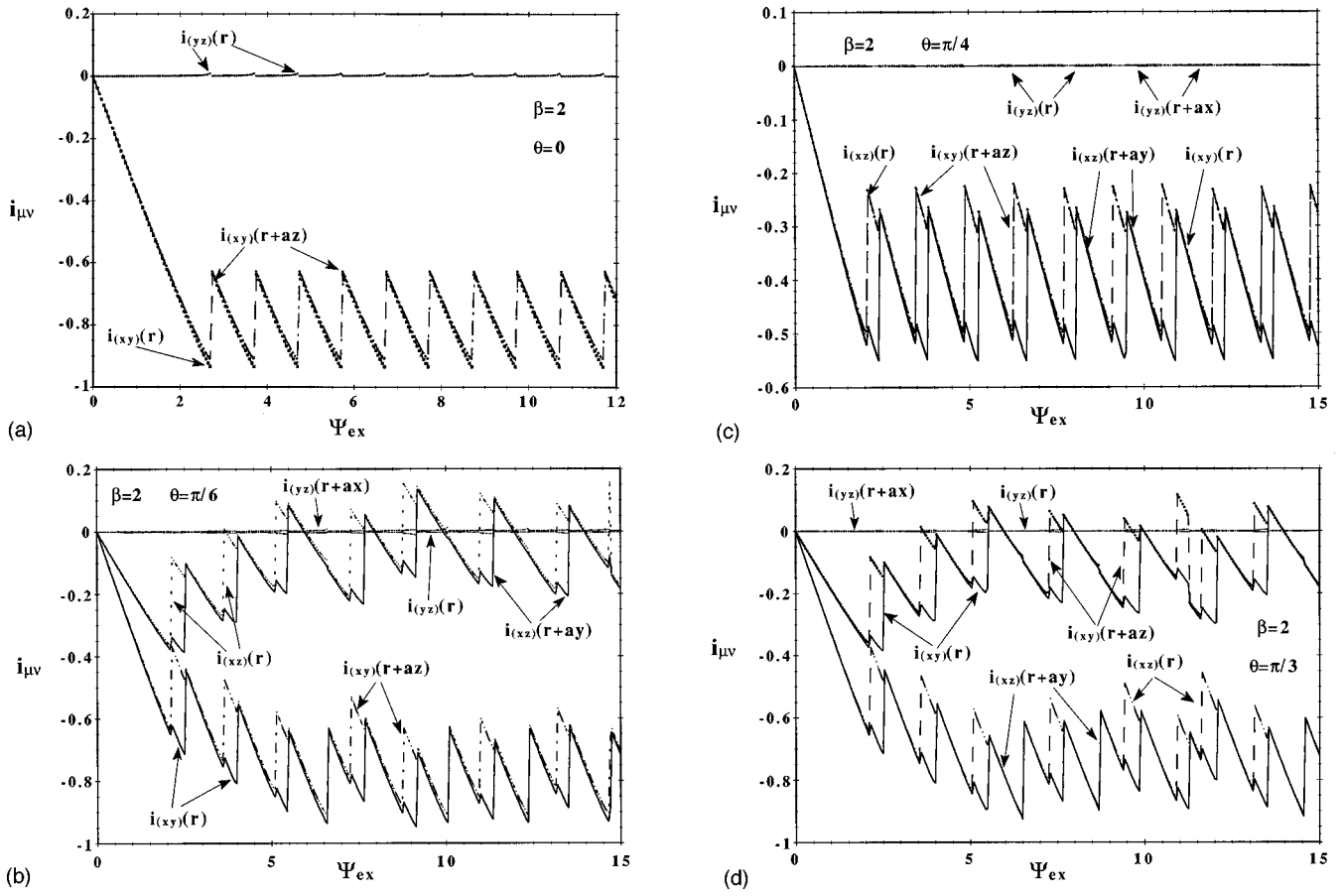

FIG. 8. Mesh currents circulating in the six cubic faces as a function of the normalized applied flux Ψ_{ex} for nonidentical junctions. The average SQUID parameter is $\beta=2.0$ and the maximum Josephson currents have a peaked distribution about the mean. Four runs have been done for the following field orientations: (a) $\theta=0$; (b) $\theta=\pi/6$; (c) $\theta=\pi/4$; (d) $\theta=\pi/3$. In Fig. 8(a) we let Ψ_{ex} increase from 0 to 12. In Figs. 8(b)–8(d) the external field is taken to increase from 0 to 15.

We may, as a second example, describe flux transitions in the case of $\theta=\pi/4$. As it can be seen from Fig. 7(c), a flux transition involving one fluxon entering the x-z face located at position $\mathbf{r}$ and exiting from the upper base face occurs at a lower field than a second transition involving another fluxon entering from the lower base face and exiting from the x-z face located at $(\mathbf{r}+a\hat{y})$. This penetration mechanism repeats with a fixed periodicity at higher fields. In order to recognize that JJ suffers phase slip during each flux transition, we may proceed as follows. First notice that the net current circulating in $JJ_x(\mathbf{r}+a\hat{z})$ is given by the adding contributions of both $i_{xz}(\mathbf{r})$ and $i_{xy}(\mathbf{r}+a\hat{z})$. The same happens for $JJ_x(\mathbf{r}+a\hat{y})$, in which the net current is given by the adding contributions of both $i_{xy}(\mathbf{r})$ and $i_{xz}(\mathbf{r}+a\hat{y})$. When the net current in one of these two junctions is close to the maximum Josephson current, a flux transition occur. Given now that $JJ_x(\mathbf{r}+a\hat{z})$ is weaker than $JJ_x(\mathbf{r}+a\hat{y})$, flux transitions in the former JJ always appear at a lower field. A similar type of reasoning can be applied in analyzing the magnetic response for other field directions.

V. LOWER THRESHOLD FIELD

In the present section we first show that, for field directions perpendicular to one of the faces of the 3D homogeneous network, a first threshold field is present for a certain range of the β parameter of the model. Then, after having analytically determined this range, we find a closed analytic expression for the lower threshold field in terms of β.

Let us consider the external field applied in a direction orthogonal to the cube base, so that $\mathbf{H}=H\hat{z}$. For symmetry reasons, the stationary solutions of Eqs. (17) are given by the following:

$$I_{J0}\sin\varphi_x=I_b, \tag{18}$$

$$I_{J0}\sin\varphi_y=-I_b, \tag{19}$$

$$I_{J0}\sin\varphi_z=0, \tag{20}$$

where $I_b>0$ is the absolute value of the current circulating in the base face and in the upper face of the cube. By making use of the current-flux relations, we can write

$$I_{(\mu\nu)}=\Phi_{(\mu\nu)}=0 \quad \text{if} \quad (\mu\nu)\neq(xy), \tag{21}$$

$$I_b=\frac{\Phi_{ex}-\Phi_b}{l+m} \quad \text{for} \quad (\mu\nu)=(xy), \tag{22}$$

where $\Phi_b=\Phi_{(xy)}(\mathbf{r})=\Phi_{(xy)}(\mathbf{r}+a\hat{z})$.

In this case we can choose one independent phase variable φ_b for all junctions lying in the base face, so that, making use of fluxoid quantization, the normalized flux Ψ_b can be written as

$$\Psi_b = \frac{2\varphi_b}{\pi}, \tag{23}$$

and the nontrivial stationary equations [Eqs. (18)–(20)] take the following form:

$$\Psi_b + \widetilde{\beta}\,\sin(\pi\Psi_b/2) = \Psi_{\mathrm{ex}}, \tag{24}$$

where $\widetilde{\beta} = I_{J0}(l+m)/\Phi_0$. The β_c value is obtained by taking the Ψ_b derivative of the above expression and by looking at the minimum value of $\widetilde{\beta}$ for which this derivative can be zero. We therefore find $\widetilde{\beta}_c = 2/\pi$. We can now find the value of the first threshold field value by solving simultaneously Eq. (24) and the equation obtained by differentiating both sides of Eq. (24) and by setting

$$\frac{d\Psi_{\mathrm{ex}}}{d\Psi_b} = 1 + \frac{\pi}{2}\,\widetilde{\beta}\,\cos\left(\frac{\pi}{2}\,\Psi_b\right) = 0, \tag{25}$$

thus obtaining

$$\Psi_{\mathrm{ex}}^{(1)} = \widetilde{\beta}\,\sqrt{1-\left(\frac{2}{\pi\widetilde{\beta}}\right)^2} + \frac{2}{\pi}\left[\pi - \sin^{-1}\sqrt{1-\left(\frac{2}{\pi\widetilde{\beta}}\right)^2}\right]. \tag{26}$$

The above equation thus defines the lower threshold field value in terms of the parameter $\widetilde{\beta}$ for the cubic network in the presence of an axial external magnetic field. A numerical evaluation of $\Psi_{\mathrm{ex}}^{(1)}$ is shown in Fig. 9 in terms of the parameter $\beta = lI_{J0}/\Phi_0$. The comparison between the numerically evaluated $\Psi_{\mathrm{ex}}^{(1)}$ vs β curve and the analytical expression in Eq. (26) shows a good agreement between the numerical and analytic solution of the problem.

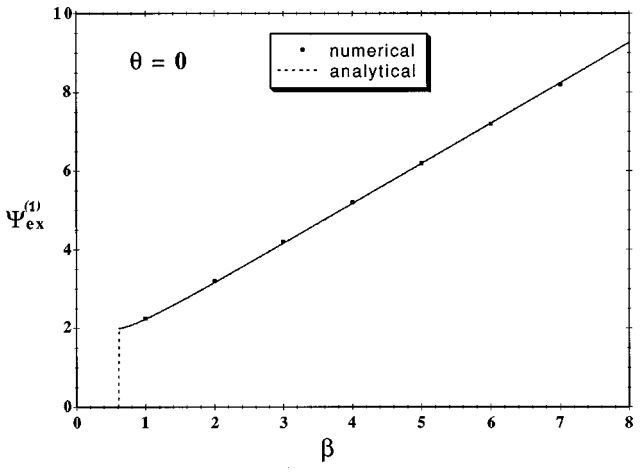

FIG. 9. Lower threshold field in the cubic network of Fig. 1 as a function of the SQUID parameter β for an axially applied external magnetic field.

VI. CONCLUSIONS

We studied the low-field response of the simplest three-dimensional Josephson junction cubic network in which the magnetic energy of the circulating currents is taken into account by introducing mutual inductance coefficients between closed loops in the networks. A characteristic parameter β, similar to the usual SQUID parameter, may be defined for this system. We estimate the value of the parameter β to be of the order of unity and take $\beta = 2$ throughout. The stationary magnetic states of the system are then obtained by numerical analysis, starting from zero-field cooling conditions and fixing the applied field direction. In general, we find that a lower threshold field value, which depends on the field direction, separates a low-field reversible region from an upper region in which irreversible flux transitions occur. Moreover, the penetration mechanisms are such to generate a flux distribution in the system which asymptotically reproduces the symmetry of the applied field. We show that, for a completely homogeneous system and for an axial applied field, the network behaves much like a simple SQUID, so that a close analytic expression for the lower threshold field can be found. Moreover, more than one fluxon are involved in a single flux transition when a homogeneous system is considered. For the inhomogeneous case, on the other hand, asymmetric states appear even for axial applied fields, and fluxons enter the network one at a time, thus producing lower steps at the points of discontinuity in which flux transitions are seen to occur in the flux distribution vs applied field curves.

Finally, the dynamical equations for the superconducting phases of the junctions are written in a general fashion, so that applications to more complex systems can be developed in future works.

[1] J. G. Bednorz and K. A. Muller, Z. Phys. B **64**, 189 (1986).
[2] J. R. Clem, Physica C **153-155**, 50 (1988).
[3] M. Tinkham and C. J. Lobb, Solid State Phys. **42**, 91 (1989).
[4] K. Nakajima and Y. Sawada, J. Appl. Phys. **52**, 5732 (1981).
[5] C. J. Lobb, D. W. Abrahams, and M. Tinkham, Phys. Rev. B **27**, 150 (1983).
[6] C. Ebner and D. Stroud, Phys. Rev. B **31**, 165 (1985).
[7] D. X. Chen, A. Sanchez, and A. Hernando, Phys. Rev. B **50**, 13 735 (1994).
[8] J. R. Phillips, H. S. J. Van der Zant, J. White, and T. P. Orlando, Phys. Rev. B **47**, 5219 (1993).
[9] T. Wolf and A. Majhofer, Phys. Rev. B **47**, 7481 (1993).
[10] J. Paasi, A. Tuohimaa, and J.-T. Eriksson, Physica C **259**, 10 (1996).
[11] R. De Luca, S. Pace, C. Auletta, and G. Raiconi, Phys. Rev. B **52**, 7474 (1995).
[12] S. P. Yukon and N. Chu H. Lin, IEEE Trans. Appl. Supercond. **5**, 2959 (1995).
[13] A. Barone and G. Paternò, *Physics and Applications of the Josephson Effect* (Wiley, New York, 1982).
[14] D. Reinel, W. Dieterich, T. Wolf, and A. Majhofer, Phys. Rev. B **49**, 9118 (1994).
[15] E. Weber, *Electromagnetic Fields* (Wiley, New York, 1954).